J. Fluid Mech. (1997), *vol.* 333, *pp.* 125–137

On the stability of attachment-line boundary layers. Part 2. The effect of leading-edge curvature

By RAY-SING LIN AND MUJEEB R. MALIK
High Technology Corporation, PO Box 7262, Hampton VA 23666, USA

(Received 17 April 1996 and in revised form 26 September 1996)

The stability of the incompressible attachment-line boundary layer has been studied by Hall, Malik & Poll (1984) and more recently by Lin & Malik (1996). These studies, however, ignored the effect of leading-edge curvature. In this paper, we investigate this effect. The second-order boundary-layer theory is used to account for the curvature effects on the mean flow and then a two-dimensional eigenvalue approach is applied to solve the linear stability equations which fully account for the effects of non-parallelism and leading-edge curvature. The results show that the leading-edge curvature has a stabilizing influence on the attachment-line boundary layer and that the inclusion of curvature in both the mean-flow and stability equations contributes to this stabilizing effect. The effect of curvature can be characterized by the Reynolds number R_a (based on the leading-edge radius). For $R_a = 10^4$, the critical Reynolds number $\bar{R}$ (based on the attachment-line boundary-layer length scale, see §2.2) for the onset of instability is about 637; however, when R_a increases to about 10^6 the critical Reynolds number approaches the value obtained earlier without curvature effect.

1. Introduction

In a swept-wing boundary layer, various instability mechanisms may initiate the transition from laminar to turbulent flow. However, evidence acquired from various experiments (cf. Maddalon *et al.* 1989) shows that maintaining a laminar attachment line is crucial to the application of laminar-flow-control technology to modern aircraft. Therefore, understanding of the attachment-line boundary-layer stability represents a problem of primary importance in the design of advanced laminar-flow-control swept wings.

The linear stability of the attachment-line boundary layer was studied by Hall, Malik & Poll (1984, hereafter referred to as HMP) ignoring the surface-curvature effect. HMP considered a special class of two-dimensional disturbances:

$$\{u', v', w'\} = \{x\hat{u}(y), \hat{v}(y), \hat{w}(y)\}\, \mathrm{e}^{\mathrm{i}[\beta z - \omega t]}, \tag{1.1}$$

where β is the spanwise wavenumber and ω is the disturbance frequency. Based on the temporal stability theory, they found the critical Reynolds number $\bar{R}$ (see §2.2) to be 583.1 (the equivalent momentum-thickness Reynolds number is about 235), which for the first time agreed well with the experimental data of Pfenninger & Bacon (1969) and Poll (1979). The validity of this special form of disturbance was later confirmed by the direct numerical simulation of Spalart (1988) and Joslin (1995). Theofilis (1995) considered the spatial stability problem using the HMP equations. The results yielded the same dominant instability studied by HMP.

Recently, Lin & Malik (1996, hereafter referred to as Part 1) developed a generalized approach for determining the stability of attachment-line boundary layers by solving the two-dimensional eigenvalue problem resulting from the linearized partial-

differential stability equations. In this approach, the restriction imposed by (1.1) is lifted; therefore, disturbances of general structure are admitted. The analysis yields global information regarding both two- and three-dimensional disturbances. As in HMP, the mean flow considered in Part 1 was swept Hiemenz flow. In Part 1 the effect of the leading-edge curvature was also ignored in the stability equations. The results of Part 1 confirmed that, in an incompressible attachment-line boundary layer, the two-dimensional disturbances described by (1.1) always have the highest growth rate and dictate the instability. They also showed, however, the existence of unstable modes in addition to the one found by HMP. In this paper, we extend the work in Part 1 to study the effect of curvature on the attachment-line boundary-layer stability.

An accurate mean-flow solution must be obtained before embarking on the task of stability analysis. In the limit of large Reynolds number, the classical first-order boundary-layer solution is considered a reasonable approximation to the solution of the Navier–Stokes equations. Within the framework of Prandtl's theory, effects of surface curvature and displacement of the external flow by the boundary layer are considered as higher-order terms and are neglected. At finite Reynolds numbers and in regions of high curvature, however, boundary-layer flows cannot be accurately treated by first-order theory. The attachment-line flow on a highly swept wing with a small leading-edge radius of curvature is one of those situations. In order to address the issue of surface curvature, Prandtl's classical boundary-layer theory is extended to include the second-order correction terms, based on the work of Gersten & Gross (1973); the extension is known as higher-order boundary-layer theory, and an excellent review on this subject has been given by Van Dyke (1969).

In order to account for the leading-edge curvature effect in the stability equations, we adopt the approach of Part 1 which solves a two-dimensional eigenvalue problem governed by partial differential equations. The effect of leading-edge curvature is fully accounted for when these equations are written in body-intrinsic coordinates.

The rest of this paper is organized as follows: in §2 we first present the second-order boundary-layer theory and a discussion of the effect of curvature on the mean flow followed by a formulation of the two-dimensional partial-differential eigenvalue problem governing the stability of general disturbances. In §3 we give the results for the effect of leading-edge curvature on stability. Some discussion on the results is given in §4. Finally, in §5 we give the conclusions.

2. Problem formulation

In this paper, our main goal is to examine the effects of leading-edge curvature on attachment-line boundary-layer stability. To adequately address this problem, the correct laminar flow must be obtained. In addition, all effects associated with the surface curvature, such as the centrifugal force and the streamline divergence, must be incorporated into the stability formulation. For small leading-edge radius, one way to obtain mean flow is to solve the Navier–Stokes equations. Alternatively, second-order boundary-layer theory can be used for flows with a leading-edge Reynolds number above a certain limit. Here, we employ the latter approach.

2.1. *Second-order boundary layer*

For three-dimensional incompressible flows near the attachment line, two kinds of second-order effects have been recognized: surface curvature (local), and displacement (global). The local effects are those determined from the inner solution only; global effects are those which require the second-order outer solution to the flow around the

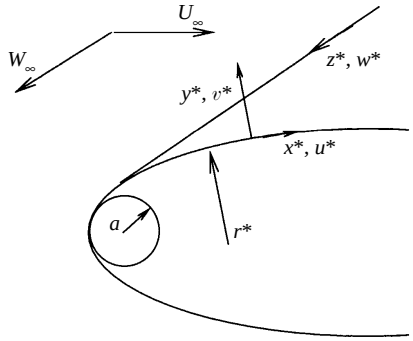

FIGURE 1. Coordinate system for attachment-line boundary-layer flow.

entire body. The second-order outer solution is tedious to obtain and often not possible for complex flows involving separation, wake, etc. Therefore, only a few higher-order boundary-layer solutions have ever been computed; for example, the uniform flow over a parabola by Van Dyke (1964*a*) and the Rankine half-body by Devan (1964). Later, Gersten & Gross (1973) extended Van Dyke's work to include the effects of sweep and mass transfer. Since the work of Gersten & Gross is most relevant to swept wings, we will use their analysis to compute the basic state for the present application. The technique of matched asymptotic expansions is used to find the higher-order approximation to the singular-perturbation problem. Here, we only give a brief description; details may be found in Van Dyke (1964*b*).

The body-intrinsic coordinate system used here is shown schematically in figure 1. The x^*-axis is taken to be the chordwise direction along the surface, the y^*-axis is in the wall-normal direction, and the z^*-axis is in the spanwise direction. The velocity components along the x^*, y^* and z^* coordinates are denoted by u^*, v^* and w^*, respectively, and the pressure is denoted by p^*. For the boundary-layer solution, we non-dimensionalize the velocities u^* and v^* with U_∞, w^* with W_∞ and pressure with ρU_∞^2. Here, ρ is the density and subscript ∞ refers to the free-stream conditions. The leading-edge sweep angle λ is given by

$$\tan\lambda = W_\infty/U_\infty. \tag{2.1}$$

The radius of curvature of the leading edge is denoted by a, while the local radius of curvature of the wall (in the chordwise direction) is indicated by $r^*(r^* \to a$ as $x^* \to 0)$. We use a as the length scale, so that $\bar{x} = x^*/a, \bar{y} = y^*/a, \bar{z} = z^*/a$. A Reynolds number R_a, which we call the leading-edge Reynolds number, is defined as

$$R_a = U_\infty a/\nu, \tag{2.2}$$

where ν is the kinematic viscosity. To construct the asymptotic expansions for the solution to the Navier–Stokes equations, the small perturbation parameter is chosen as

$$\epsilon = 1/R_a^{1/2}. \tag{2.3}$$

Outer expansions

We assume that the outer expansions of the solutions are in the following form:

$$u^*/U_\infty = U_1(\bar{x},\bar{y}) + \epsilon U_2(\bar{x},\bar{y}) + \dots, \tag{2.4a}$$

$$v^*/U_\infty = V_1(\bar{x},\bar{y}) + \epsilon V_2(\bar{x},\bar{y}) + \dots, \tag{2.4b}$$

$$w^*/W_\infty = W_1(\bar{x},\bar{y}) + \epsilon W_2(\bar{x},\bar{y}) + \dots, \tag{2.4c}$$

$$(p^* - p_\infty)/\rho U_\infty^2 = P_1(\bar{x},\bar{y}) + \epsilon P_2(\bar{x},\bar{y}) + \dots. \tag{2.4d}$$

Geometry	U_{11}	U_{21}	Reference
Parabola	1	−0.61	Van Dyke (1964*a*)
Rankine body	1.5	−0.62	Devan (1964)

TABLE 1. First and second outer solutions near the leading edge

Substituting these expressions into the steady Navier–Stokes equations and collecting terms of the same order yields a sequence of systems of equations. It is observed that up to $O(\epsilon^2)$ viscous effects do not appear. Thus, outer solutions of first and second order correspond to inviscid flows.

With a uniform-flow upstream, the first-order outer expansion represents a potential flow whose solution leads to the Bernoulli equation:

$$P_1(\bar{x},0) = \tfrac{1}{2} - \tfrac{1}{2}(U_1^2(\bar{x},0) + V_1^2(\bar{x},0)). \tag{2.5}$$

The above equation defines the wall pressure P_1 when U_1 and V_1 are known. The boundary conditions that the first-order solution must satisfy are:

$$\bar{y} = 0, \quad V_1(\bar{x},0) = 0, \tag{2.6a}$$

$$\bar{y} \to \infty, \quad U_1^2 + V_1^2 = 1. \tag{2.6b}$$

Similarly, the solution of the second-order outer expansion also leads to an equation analogous to (2.5):

$$P_2 + U_1 U_2 + V_1 V_2 = 0. \tag{2.7}$$

The boundary conditions at the wall for the outer expansions are determined by matching with the inner solution. The boundary condition for $V_2(\bar{x},0)$ turns out to be:

$$V_2(\bar{x},0) = [U_{11}\beta_1]^{1/2}, \tag{2.8}$$

where U_{11} and β_1 are constants which will be defined later. For the spanwise velocity component, the first and second outer solutions are simply

$$W_1 = 1, \quad W_2 = 0. \tag{2.9a, b}$$

Since only the solutions near the attachment line are of interest here, the solution for u^* on the wall can be further expanded for small values of $\bar{x}$:

$$\frac{u^*(\bar{x},0)}{U_\infty} = U_{11}\bar{x} + U_{13}\bar{x}^3 + \ldots + \epsilon(U_{21}\bar{x} + U_{23}\bar{x}^3 + \ldots)$$

$$= U_{11}\bar{x}\left(1 + \frac{U_{21}}{U_{11}}\epsilon + \ldots\right). \tag{2.10}$$

The coefficient for the first-order velocity, U_{11}, is a constant which depends on the geometry of the body. The coefficient for the second-order velocity, U_{21}, is also a constant which depends only on the displacement effect of the first-order inner solution. Their values are available for two bodies, as listed in table 1. Note that Davis (1972) performed Navier–Stokes computations for a parabolic cylinder and his skin-friction results agreed with those obtained by Van Dyke (1964*a*) at $R_a \geqslant 10^4$.

It is also worth noting that the determination of the coefficient U_{21} involves the global solution to the potential flow over the effective body which consists of the solid body and the displacement thickness. In general, for a closed body, it is almost impossible to find this coefficient, since the separation and the wake can have a profound effect on the effective body.

Inner expansions

For solutions in the boundary layer, the normal coordinate $\bar{y}$ is replaced by a stretched inner variable

$$\eta = \bar{y}/\epsilon. \tag{2.11}$$

The inner solutions are formulated such that the continuity equation is satisfied automatically, similar to the formulation of the Falkner–Skan family. The first term in each equation is the first-order approximation and the last two terms represent the second-order approximation. The first of these latter two terms represents the curvature effect which is the subject of our investigation, and the second is the displacement-effect term. The inner expansions are as follows:

$$u^*/U_\infty = \bar{x}[f'(\eta)+\epsilon F_c'(\eta)+\epsilon U_{21} F_d'(\eta)+\dots], \tag{2.12a}$$

$$v^*/U_\infty = \frac{-\epsilon}{1+\bar{y}}[f(\eta)+\epsilon F_c(\eta)+\epsilon U_{21} F_d(\eta)+\dots], \tag{2.12b}$$

$$w^*/W_\infty = h(\eta)+\epsilon H_c(\eta)+\epsilon U_{21} H_d(\eta)+\dots, \tag{2.12c}$$

$$(p^*-p_\infty)/\rho U_\infty^2 = \tfrac{1}{2}-\tfrac{1}{2}\bar{x}^2[p(\eta)+\epsilon P_c(\eta)+\epsilon U_{21} P_d(\eta)+\dots]. \tag{2.12d}$$

Substituting these expressions into the Navier–Stokes equations and collecting terms of the same order of ϵ, yields the following set of ordinary differential equations.

The equations for u^* are:

$$f'''+ff''+p-f'^2 = 0, \tag{2.13a}$$

$$F_c'''+fF_c''-2f'F_c'+f''F_c = -P_c-\eta f'''-f''-ff', \tag{2.13b}$$

$$F_d'''+fF_d''-2f'F_d'+f''F_d = -P_d. \tag{2.13c}$$

The equations for w^* are:

$$h''+fh' = 0, \quad H_c''+fH_c' = (\eta f-1-F_c)h', \quad H_d''+fH_d' = -F_d h'. \tag{2.14a–c}$$

The equations for p^* are:

$$p' = 0, \quad P_c' = -2f'^2, \quad P_d' = 0. \tag{2.15a–c}$$

The far-field ($\eta \to \infty$) boundary conditions are determined by direct matching. The detailed matching procedure will not be given here but can be found in Gersten & Gross (1973). The results of the asymptotic matching at $\eta \to \infty$ and the physical considerations at $\eta = 0$ yield boundary conditions for the above system of ordinary differential equations. They are:

for $\eta = 0$

$$f = 0, \quad f' = 0, \quad F_c = 0, \quad F_c' = 0, \quad F_d = 0, \quad F_d' = 0, \tag{2.16a}$$

$$h = 0, \quad H_c = 0, \quad H_d = 0; \tag{2.16b}$$

and $\eta \to \infty$

$$f' = 1, \quad F_c'' = -1, \quad F_d' = 1, \quad h = 1, \quad H_c = 0, \quad H_d = 0, \tag{2.17a}$$

$$p = 1, \quad P_c = -2\eta, \quad P_d = 2. \tag{2.17b}$$

From the boundary conditions and governing equations, one obtains the following analytical solutions for pressure:

$$p = 1, \quad P_c = -\beta_1-\eta-f''-ff', \quad P_d = 2, \tag{2.18a–c}$$

where

$$\beta_1 = \lim_{\eta\to\infty}(\eta-f). \tag{2.18d}$$

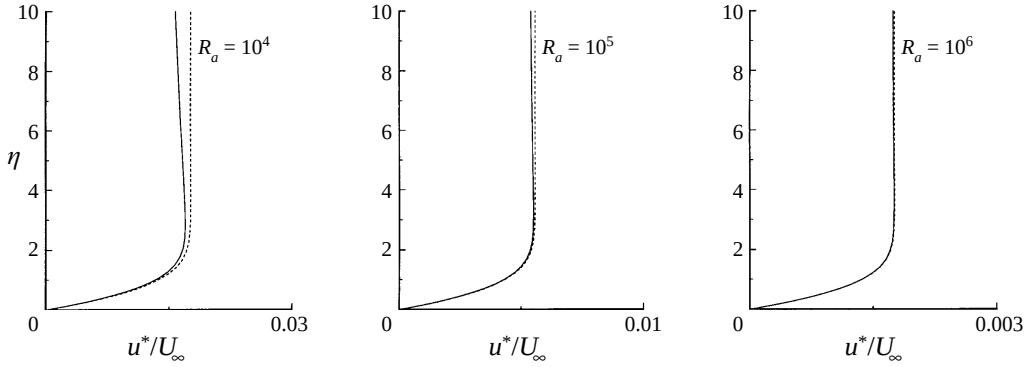

FIGURE 2. Comparison of first- and second-order chordwise velocity profiles for $R_a = 10^4$, 10^5, and 10^6. First-order: dashed; second-order: solid.

f''	1.232588	h'	0.570465
β_1	0.647900	H_c'	−0.160182
F_c''	−1.913256	H_d'	0.285233
F_d''	1.848881		

TABLE 2. Function values of the inner expansions at the wall

We solve the above system of equations, (2.13)–(2.15), with prescribed boundary conditions, (2.16)–(2.17), by Runge–Kutta integration coupled with Newton's iterations. Table 2 gives f'', F_c'', F_d'' and associated quantities on the wall. These values agree with those reported by Gersten & Gross (1973).

In figure 2, comparisons for the chordwise velocity profile (u^*/U_∞) between the classical swept-Hiemenz (first-order) solution and the second-order solution are made for three different leading-edge Reynolds numbers, $R_a = 10^4$, 10^5 and 10^6. It is clear that the difference between the first- and second-order solution increases as the leading-edge Reynolds number decreases. This indicates that the effect of surface curvature becomes stronger as the leading-edge Reynolds number, R_a, becomes smaller. It is also noticed (not given here) that the effect of curvature leads to decreasing values of wall shear stress. This behaviour results from the stretching of the boundary layer in the direction normal to the wall by centrigual forces due to the convex surface curvature. In the next subsection, we will investigate how this convex surface curvature affects the stability of the attachment-line boundary layer.

2.2. *Stability equations*

With the mean flow computed, we will now proceed to develop the theoretical framework for the investigation of the attachment-line boundary-layer stability. To do that, we rescale all the velocity components by W_∞. Thus, the mean flow whose stability is the subject of this paper is given by $\bar{Q} = (\bar{U}, \bar{V}, \bar{W}, \bar{P})$ where

$$\bar{U} = \frac{u^*}{W_\infty}, \quad \bar{V} = \frac{v^*}{W_\infty}, \quad \bar{W} = \frac{w^*}{W_\infty}, \quad \bar{P} = \frac{p^*}{\rho W_\infty^2}. \tag{2.19a–d}$$

We consider a general infinitesimal disturbance propagating along the attachment line, so that the instantaneous flow quantities can be expressed as:

$$q(x, y, z, t) = \bar{Q}(x, y) + q'(x, y, z, t), \tag{2.20}$$

where $q' = (u', v', w', p')$ represents the disturbance. We non-dimensionalize the disturbance velocity components (u', v', w') by W_∞ and p' by ρW_∞^2. The length scale is chosen as:

$$\Delta = (a\nu/U_\infty U_{11})^{1/2}. \tag{2.21}$$

Thus,
$$x = x^*/\Delta, \quad y = y^*/\Delta, \quad z = z^*/\Delta \tag{2.22}$$

and
$$r = r^*/\Delta. \tag{2.23}$$

Substituting (2.20) into the incompressible Navier–Stokes equations, subtracting the basic-state information, and linearizing with respect to small perturbations, we obtain a set of linearized stability equations.

Without making any further assumptions, the resuting problem consists of a set of coupled three-dimensional partial-differential equations with variable coefficients. For an infinite swept wing, these coefficients, which depend on the basic flow, change strongly in both the wall-normal (y) and the chordwise (x) directions, but not in the spanwise (z) direction. Consequently, the solutions are separable in the variables z and t, and can be expressed in the form:

$$q'(x, y, z, t) = \hat{q}(x, y)\, \mathrm{e}^{\mathrm{i}[\beta z - \omega t]} + \text{c.c.} \tag{2.24}$$

where c.c. represent complex conjugate. Under this normal-mode assumption, the set of non-dimensional linear stability equations can be written as:

$$\frac{r}{r+y}\frac{\partial \hat{u}}{\partial x} + \frac{\partial \hat{v}}{\partial y} + \frac{\hat{v}}{r+y} + \mathrm{i}\beta\hat{w} = 0, \tag{2.25}$$

$$\begin{aligned} -\mathrm{i}\omega\hat{u} + \frac{r}{r+y}\bar{U}\frac{\partial \hat{u}}{\partial x} + \frac{r}{r+y}\hat{u}\frac{\partial \bar{U}}{\partial x} + \bar{V}\frac{\partial \hat{u}}{\partial y} + \hat{v}\frac{\partial \bar{U}}{\partial y} + \frac{\bar{V}}{r+y}\hat{u} + \frac{\bar{U}}{r+y}\hat{v} + \mathrm{i}\beta\bar{W}\hat{u} \\ = -\frac{r}{r+y}\frac{\partial \hat{p}}{\partial x} + \frac{1}{\bar{R}}\left\{\left(\frac{r}{r+y}\right)^2\frac{\partial^2\hat{u}}{\partial x^2} + \frac{ry}{(r+y)^3}\frac{\mathrm{d}r}{\mathrm{d}x}\frac{\partial \hat{u}}{\partial x} + \frac{\partial^2\hat{u}}{\partial y^2} + \frac{1}{r+y}\frac{\partial \hat{u}}{\partial y}\right. \\ \left. + \frac{2r}{(r+y)^2}\frac{\partial \hat{v}}{\partial x} - \frac{r}{(r+y)^3}\frac{\mathrm{d}r}{\mathrm{d}x}\hat{v} - \frac{\hat{u}}{(r+y)^2} - \beta^2\hat{u}\right\}, \end{aligned} \tag{2.26}$$

$$\begin{aligned} -\mathrm{i}\omega\hat{v} + \frac{r}{r+y}\bar{U}\frac{\partial \hat{v}}{\partial x} + \frac{r}{r+y}\hat{u}\frac{\partial \bar{V}}{\partial x} + \bar{V}\frac{\partial \hat{v}}{\partial y} + \hat{v}\frac{\partial \bar{V}}{\partial y} - \frac{2\bar{U}}{r+y}\hat{u} + \mathrm{i}\beta\bar{W}\hat{v} = -\frac{\partial \hat{p}}{\partial y} + \frac{1}{\bar{R}}\left\{\left(\frac{r}{r+y}\right)^2\frac{\partial^2\hat{v}}{\partial x^2}\right. \\ \left. + \frac{ry}{(r+y)^3}\frac{\mathrm{d}r}{\mathrm{d}x}\frac{\partial \hat{v}}{\partial x} + \frac{\partial^2\hat{v}}{\partial y^2} + \frac{1}{r+y}\frac{\partial \hat{v}}{\partial y} - \frac{2r}{(r+y)^2}\frac{\partial \hat{u}}{\partial x} + \frac{r}{(r+y)^3}\frac{\mathrm{d}r}{\mathrm{d}x}\hat{u} - \frac{\hat{v}}{(r+y)^2} - \beta^2\hat{v}\right\}, \end{aligned} \tag{2.27}$$

$$\begin{aligned} -\mathrm{i}\omega\hat{w} + \frac{r}{r+y}\bar{U}\frac{\partial \hat{w}}{\partial x} + \frac{r}{r+y}\hat{u}\frac{\partial \bar{W}}{\partial x} + \bar{V}\frac{\partial \hat{w}}{\partial y} + \hat{v}\frac{\partial \bar{W}}{\partial y} + \mathrm{i}\beta\bar{W}\hat{w} \\ = -\mathrm{i}\beta\hat{p} + \frac{1}{\bar{R}}\left\{\left(\frac{r}{r+y}\right)^2\frac{\partial^2\hat{w}}{\partial x^2} + \frac{ry}{(r+y)^3}\frac{\mathrm{d}r}{\mathrm{d}x}\frac{\partial \hat{w}}{\partial x} + \frac{\partial^2\hat{w}}{\partial y^2} + \frac{1}{r+y}\frac{\partial \hat{w}}{\partial y} - \beta^2\hat{w}\right\}. \end{aligned} \tag{2.28}$$

The Reynolds number $\bar{R}$ is defined as:

$$\bar{R} = W_\infty \Delta/\nu. \tag{2.29}$$

Combining (2.1) and (2.2) with (2.29) yields

$$\bar{R} = R_a^{1/2}\tan\lambda/U_{11}^{1/2}. \tag{2.30}$$

Note that (2.25)–(2.28) are a set of two-dimensional partial-differential equations in the (x, y)-plane. This is the set of equations which best describes the stability characteristics of small perturbations because these equations fully incorporate the effects of streamline divergence and surface curvature. We note that while the above stability equations are valid at all non-zero values of $\bar{R}$ and R_a, the mean flow computed in §2.1 is valid only for $R_a \gg 1$.

The boundary conditions for (2.25)–(2.28) in the y-direction are:

$$\hat{u} = \hat{v} = \hat{w} = 0 \quad \text{at} \quad y = 0, \quad \text{and as} \quad y \to \infty. \tag{2.31}$$

In the x-direction, the boundary conditions are prescribed at $x = 0$ and $|x| = x_{max}$. Here, two types of solutions are possible: symmetric and antisymmetric. In Part 1, it was shown that symmetric modes are more unstable and only these modes will be considered in this paper. For symmetric modes, the boundary conditions are:

$$\frac{\partial \hat{w}}{\partial x} = \frac{\partial \hat{v}}{\partial x} = \hat{u} = 0, \quad x = 0, \tag{2.32a}$$

$$\hat{u}(x, y) = -\hat{u}(-x, y), \quad \hat{v}(x, y) = \hat{v}(-x, y), \quad \hat{w}(x, y) = \hat{w}(-x, y), \quad x = x_{max}. \tag{2.32b}$$

For computational purposes, the semi-infinite domain in y is truncated at $y = y_{max}$, and $y_{max} = 20\delta$ is found adequate for the least-stable mode considered here and is used throughout this paper. Similarly, the physical domain in the x-direction is truncated at $|x| = x_{max}$. The selection of x_{max} may appear to be arbitrary. However, based upon numerical experiments, it was shown in Part 1 that as long as x_{max} is greater than 2δ, a domain-independent converged solution can be achieved.

Equations (2.25)–(2.28) along with the boundary conditions (2.31)–(2.32) constitute a partial-differential eigenvalue problem which we solve by using a double Chebyshev-collocation method. In the discrete sense, a temporal eigenvalue problem can be represented as a generalized algebraic eigenvalue problem of the form

$$\boldsymbol{A}\boldsymbol{x} = \omega \boldsymbol{B}\boldsymbol{x}, \tag{2.33}$$

where $\boldsymbol{A}$ is a complex non-Hermitian matrix and $\boldsymbol{B}$ is a diagonal matrix. The order of the matrices is $2N_y N_x$, where N_y and N_x are the number of collocation points in the y- and x-directions, respectively. The above eigenvalue problem can be solved by the QR algorithm which yields all the eigenvalues of the discretized system. It may be noted that, by including the effect of curvature, the order of matrices $\boldsymbol{A}$ and $\boldsymbol{B}$ does not increase from that in Part 1. Therefore, the eigenvalue problem can be solved in the same amount of computer time with and without curvature.

3. Stability results

This section contains results of linear stability calculations using different order boundary-layer solutions and different stability formulations. To demonstrate the effect of surface curvature, the following comparisons are made at $\bar{R} = 700$:

(i) first-order boundary layer (swept Hiemenz flow), Cartesian coordinates (x, y, z), $R_a = \infty$;
(ii) second-order boundary layer, body-intrinsic coordinates (body), $R_a = 10^6$;
(iii) same as (ii), except $R_a = 10^5$;
(iv) same as (ii), except $R_a = 10^4$.

We first note from (2.30) that R_a and $\bar{R}$ can be independently varied. Varying R_a,

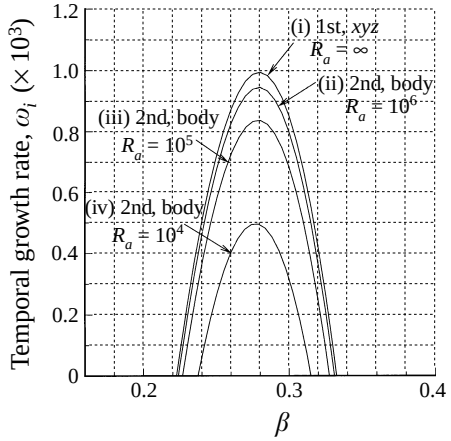

FIGURE 3. Comparison of temporal growth rates for $\bar{R} = 700$, and $R_a = \infty$, 10^6, 10^5, and 10^4.

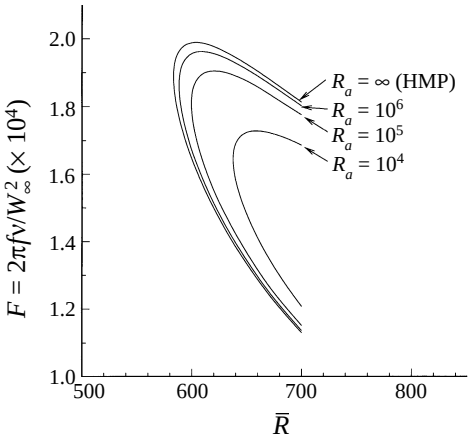

FIGURE 4. Effect of surface curvature on neutral curves.

while holding $\bar{R}$ fixed, implies that the sweep angle in (2.1) is being varied. In figure 3, temporal growth rates are plotted *vs*. the spanwise wavenumber β of the most unstable two-dimensional travelling disturbances. The difference between curves (i) and (ii), (iii), (iv) clearly shows that the effect of surface curvature is *stabilizing*. As one would expect, when R_a increases, the stability results approach that of the swept-Hiemenz flow. The difference between curves (i) and (iv) is substantial: the maximum growth rate of curve (iv) is 50 % of that of curve (i).

To illustrate the stabilizing effect of convex surface curvature on the critical Reynolds number, the neutral curves associated with the two-dimensional travelling mode are computed and are given in figure 4 for the leading-edge Reynolds numbers R_a of 10^4, 10^5, 10^6, and ∞ (swept Hiemenz flow). The critical Reynolds numbers from these curves are listed in table 3.

The increase in the critical Reynolds number is about 10 % for R_a changing from infinite to 10^4. Further reducing the leading-edge Reynolds number might produce an even higher critical Reynolds nubmer; however, the accuracy of the second-order boundary-layer theory itself may become questionable. For even lower leading-edge Reynolds-number (R_a) flows, to obtain an accurate basic state, one might have to

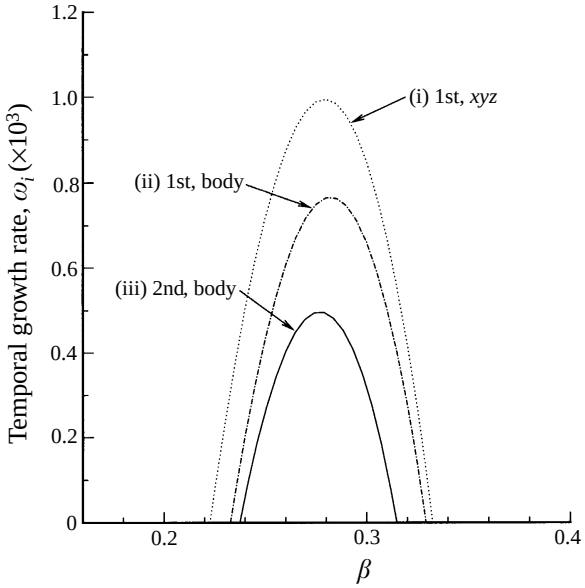

FIGURE 5. Temporal growth rate computed by different strategies for $\bar{R} = 700$, $R_a = 10^4$.

	R_a	BL order	Coordinate	Crit. $\bar{R}$
(i)	∞	First	xyz	583.1
(ii)	10^6	Second	Body	588.2
(iii)	10^5	Second	Body	599.5
(iv)	10^4	Second	Body	637.6

TABLE 3. Effect of convex leading-edge curvature on attachment-line critical Reynolds number, $\bar{R}$

appeal to a boundary-layer theory including even higher-order corrections, or, in a more practical sense, to the direct Navier–Stokes calculation.

To delineate the overall effect of curvature coming from mean flow and stability equations, a comparison of solutions using different approximations is made in figure 5. These calculations are performed based on the following different strategies: (i) 1st-xyz: the first-order boundary-layer solution is taken as the basic state and the stability equations are cast in the Cartesian coordinate system, i.e. the curvature effects are totally ignored; (ii) 1st-body: the curvature effect is retained in the stability equations only, see (2.25)–(2.28), although the first-order basic state is used; (iii) second-body: the curvature effects are fully incorporated into both the basic state and the stability analysis. Of course, as one would expect, strategy (iii) would ultimately give the most accurate results. The comparison shows that even without the second-order boundary-layer solutions, the error associated with the stability analyses can be reduced by performing the analysis using the stability formulation of (2.25)–(2.28).

4. Discussion

In (2.25)–(2.28), it is noticed that the surface curvature appears explicitly in two distinct forms: $r/(r+y)$ and $1/(r+y)$. In order to distinguish the stabilizing contribution made by various curvature terms, we manipulate the stability equations

Variation	ω_r	$\omega_i \times 10^3$
(i)	0.100797	0.4941
(ii)	0.100801	0.4944
(iii)	0.101799	0.7153
(iv)	0.101802	0.7158
(v)	0.101802	0.7158

TABLE 4. Comparison for stability calculations for $\beta = 0.275$, $R_a = 10^4$ with different variations, defined in the text

Equation	ω_r	$\omega_i \times 10^3$
continuity	0.101775	0.6984
x-momentum	0.100792	0.5002
y-momentum	0.100797	0.4957
all equations	0.101799	0.7153

TABLE 5. Effect of setting $1/(r+y) = 0$ in the stability equations ($\beta = 0.275$, $R_a = 10^4$)

systematically and perform a series of calculations in both body-intrinsic and Cartesian coordinates. Calculations are conducted for a wavenumber of 0.275 with a fixed boundary-layer solution at $R_a = 10^4$. A comparison is made for calculations with following variations:

(i) body-intrinsic coordinates + full set of equations (no variations),
(ii) body-intrinsic coordinates + set $r/(r+y) \to 1$ only,
(iii) body-intrinsic coordinates + set $1/(r+y) \to 0$ only,
(iv) body-intrinsic coordinates + set $r/(r+y) \to 1$ and $1/(r+y) \to 0$,
(v) Cartesian coordinates (equations of Part 1).

Results of these calculations are summarized in table 4. As expected, by letting both $r/(r+y) \to 1$ and $1/(r+y) \to 0$ as in case (iv), the result of case (v) (stability equations of Part 1) is fully recovered. The differences in growth rates given in table 4 clearly show that the prime stabilizing curvature effect comes from terms associated with $1/(r+y)$. Among these terms, only those appearing in the inviscid part of the momentum equations and continuity equation can be expected to contribute to the stabilization effect found here. An order-of-magnitude analysis for the Görtler problem (Hall 1983) shows that only the centrifugal acceleration term $2\bar{U}\hat{u}/(r+y)$ in the normal momentum equation gives rise to the Görtler instability on a concave wall. Masad & Malik (1994) found that this same term produces the dominant stabilizing effect of convex surface curvature on crossflow instability. However, since the attachment-line problem is focused on a region of small x, $\bar{U}$ is small; consequently, $2\bar{U}\hat{u}/(r+y)$ is a small term and should not be the main contributing term to the stabilizing effect found above. In order to understand this stabilizing effect, we give in table 5 results of calculations done by letting $1/(r+y) \to 0$ in each of the continuity, x-momentum, and y-momentum equations in turn. The difference between these results shows that the dominant stabilizing curvature effect comes from the $\hat{v}/(r+y)$ term in the continuity equation, and the centrifugal acceleration terms in both the x- and y-momentum equations (2.26)–(2.27) have very little influence on the stability. It follows that, for $R_a \gg 1$, all curvature terms can be dropped except the one appearing in the continuity equation. An order-of-magnitude analysis of (2.25)–(2.28) may also reach

the same conclusion. However, as pointed out earlier, keeping all the terms does not increase the computational effort.

Now we discuss the practical implications of our results. Assuming an aircraft flying at a unit Reynolds number of about 2×10^6/ft, with a wing sweep angle of 30° and a leading-edge radius of about 4 in., the leading-edge Reynolds number R_a will be about 5.8×10^5. Based on the results presented above, the effect of leading-edge curvature will be small. For the conditions of Poll's (1979) experiment, $R_a \approx 4 \times 10^5$, and this is why the results of HMP are in good agreement with the experimental results. However, for supersonic aircraft with small leading edge, this effect may not be negligible.

On a tapered swept wing, the leading-edge radius of curvature a decreases from the root to the tip. As a result, the attachment-line Reynolds number $\bar{R}$ will also decrease from the wing–fuselage juncture to the outboard section of the wing. On the other hand, as shown above, the critical Reynolds number will become higher at the outboard section. The combined effect might inhibit, or even reverse the transition process. In the context of leading-edge contamination, the phenomenon of reverse transition has been observed by Poll & Paisley (1985) in their wind tunnel experiments on a tapered model.

5. Conclusions

This paper addresses issues related to the incompressible attachment-line boundary-layer stability using a two-dimensional eigenvalue approach. The stability equations are kept in the partial-differential form and are written in a body-intrinsic coordinate system; thus the effects of the streamline divergence and surface curvature are exactly formulated. The effect of leading-edge curvature in the mean flow is accounted for in the framework of second-order boundary-layer theory.

Results indicate that the effect of leading-edge curvature is stabilizing. The critical Reynolds number gradually increases as R_a (Reynolds number based on leading-edge radius) decreases. The reduction in R_a can be achieved either by using a smaller leading-edge radius or by increasing sweep; however, increasing the sweep angle enhances the crossflow instability as well as the Reynolds number $\bar{R}$ based on W_∞ and Δ. It is also found that the main stabilizing effect of curvature comes from the perturbation equation for conservation of mass and not momentum.

This work was supported by National Aeronautics and Space Administration under NASA Contracts NAS1-19299 and NAS1-20059.

REFERENCES

Davis, R. T. 1972 Numerical solution of the Navier–Stokes equations for symmetric laminar incompressible flow past a parabola. *J. Fluid Mech.* **51**, 417.

Devan, L. 1964 Second order incompressible laminar boundary layer development on a two dimensional semi-infinite body. PhD thesis, University of California at Los Angeles.

Gersten, K. & Gross, J. F. 1973 Mass-transfer effects on higher-order boundary layer solutions: The leading edge of a swept cylinder. *Intl J. Heat Mass Transfer* **16**, 65.

Hall, P. 1983 The linear development of Görtler vortices in growing boundary layer. *J. Fluid Mech.* **130**, 41.

Hall, P., Malik, M. R. & Poll, D. I. A. 1984 On the stability of an infinite swept attachment line boundary layer. *Proc. R. Soc. Lond.* A **395**, 229 (referred to herein as HMP).

Joslin, R. D. 1995 Direct simulation of evolution and control of three-dimensional instabilities in attachment-line boundary layers. *J. Fluid Mech.* **291**, 369.

LIN, R.-S. & MALIK, M. R. 1996 On the stability of attachment-line boundary layers. Part 1. The incompressible swept Hiemenz flow. *J. Fluid Mech.* **311**, 239 (referred to herein as Part 1).

MASAD, J. A. & MALIK, M. R. 1994 Effects of body curvature and nonparallelism on the stability of flow over a swept cylinder. *Phys. Fluids* **6**, 2363.

MADDALON, D. V., COLLIER, F. S., MONTOYA, L. C. & LAND, C. K. 1989 Transition flight experiments on a swept wing with suction. *AIAA Paper* 89-1893.

PFENNINGER, W. & BACON, J. W. 1969 Amplified laminar boundary layer oscillations and transition at the front attachment line of a 45 flat-nosed wing with and without boundary layer suction. In *Viscous Drag Reduction* (ed. C. S. Wells). Plenum.

POLL, D. I. A. 1979 Transition in the infinite swept attachment line boundary layer. *Aero Q* **30**, 607.

POLL, D. I. A. & PAISLEY, D. J. 1985 On the effect of wing taper and sweep direction on leading edge transition. *Aero. J.* March, 109.

SPALART, P. R. 1988 Direct numerical study of leading-edge contamination. In *AGARD Conf. Proc.* 438, *Fluid Dynamics of Three-Dimensional Turbulent Shear Flows and Transition*, *Cesme*, *Turkey*, pp 5-1–5-13.

THEOFILIS, V. 1995 Spatial stability of incompressible attachment-line flow. *Theoret. Comput. Fluid Dyn.* **7**, 159.

VAN DYKE, M. 1964*a* Higher approximations in boundary layer theory. Part 3. Parabola in uniform stream. *J. Fluid Mech.* **19**, 145.

VAN DYKE, M. 1964*b* *Perturbation Methods in Fluid Mechanics*. Academic.

VAN DYKE, M. 1969 Higher-order boundary-layer theory. *Ann. Rev. Fluid Mech.* **1**, 265.